Genetic associations of serum accumulation of PFASs and their impacts on brain structure and mental health

Authors names and affiliations: Jiayuan Xu[1,#], Xiaojun Xu[2,#], Zhihan Yan[3,#], Longjiang Zhang[4], Jingliang Cheng[5], Wenzhen Zhu[6], Shijun Qiu[7], Zuojun Geng[8], Yongqiang Yu[9], Weihua Liao[10,11,12], Hui Zhang[13], Bo Gao[14,15], Tong Han[16], Zhenwei Yao[17], Quan Zhang[18], Wen Qin[1], Feng Liu[1], Meng Liang[19], Junping Wang[1], Quan Zhang[1], Hao Ding[19], Jie Tang[1], Yuan Ji[1], Qian Qian[1], Yujie Zhang[1], Nana Liu[1], Qiang Xu[1], Jilian Fu[1], Yao Zhou[20], Huaigui Liu[1], Mulin Jun Li[20], Caihong Wang[5], Peng Zhang[21], Wei Li[21], Wei Wei[22], Dapeng Shi[22], Su Lui[23,24], Feng Chen[25], Jing Zhang[26,27], Wen Shen[28], Yanwei Miao[29], Dawei Wang[30], Jia-Hong Gao[31], Yunjun Yang[32], Kai Xu[33], Junfang Xian[34], Bing Zhang[35], Zhaoxiang Ye[21], Xiaochu Zhang[36], Xi-Nian Zuo[37,38], Liping Yang[39], Guangbin Cui[40,*], Meiyun Wang[22,41,*], Chunshui Yu[1,19,*] and the CHIMGEN Consortium

[1]Department of Radiology, Tianjin Key Lab of Functional Imaging and State Key Laboratory of Experimental Hematology, Tianjin Medical University General Hospital, 300052 Tianjin, China
[2]Department of Radiology, The Second Affiliated Hospital of Zhejiang University, School of Medicine, 310009 Hangzhou, China
[3]Department of Radiology, The Second Affiliated Hospital and Yuying Children's Hospital of Wenzhou Medical University, 325027 Wenzhou, China
[4]Department of Radiology, Jinling Hospital, Affiliated Hospital of Medical School, Nanjing University, 210002 Nanjing, China
[5]Department of Magnetic Resonance Imaging, The First Affiliated Hospital of Zhengzhou University, 450052 Zhengzhou, China
[6]Department of Radiology, Tongji Hospital, Tongji Medical College, Huazhong University of Science and Technology, 430030 Wuhan, China
[7]Department of Medical Imaging, The First Affiliated Hospital of Guangzhou University of Traditional Chinese Medicine, 510405 Guangzhou, China
[8]Department of Medical Imaging, The Second Hospital of Hebei Medical University, 050000 Shijiazhuang, China
[9]Department of Radiology, The First Affiliated Hospital of Anhui Medical University, 230022 Hefei, China
[10]Department of Radiology, Xiangya Hospital, Central South University, 410008 Changsha, China
[11]Molecular Imaging Research Center of Central South University, 410008 Changsha, China

[12]National Clinical Research Center for Geriatric Disorders, Xiangya Hospital, Central South University, 410008 Changsha, China
[13]Department of Radiology, The First Hospital of Shanxi Medical University, 030001 Taiyuan, China
[14]Department of Radiology, The Affiliated Hospital of Guizhou Medical University, 550004 Guiyang, China
[15]Department of Radiology, Yantai Yuhuangding Hospital, 264000 Yantai, China
[16]Department of Radiology, Tianjin Huanhu Hospital, 300350 Tianjin, China
[17]Department of Radiology, Huashan Hospital, Fudan University, 200040 Shanghai, China
[18]Department of Radiology, Characteristic Medical Center of Chinese People's Armed Police Force, 300162 Tianjin, China
[19]School of Medical Imaging and Tianjin Key Laboratory of Functional Imaging, Tianjin Medical University, 300203 Tianjin, China
[20]Department of Pharmacology, The Province and Ministry Co-sponsored Collaborative Innovation Center for Medical Epigenetics, Tianjin Key Laboratory of Inflammatory Biology, School of Basic Medical Sciences, Tianjin Medical University, 300203 Tianjin, China
[21]Department of Radiology, Tianjin Medical University Cancer Institute & Hospital, National Clinical Research Center for Cancer, Tianjin's Clinical Research Center for Cancer, Tianjin Medical University, Ministry of Education, Key Laboratory of Cancer Prevention and Therapy, 300060 Tianjin, China
[22]Department of Radiology, Henan Provincial People's Hospital & Zhengzhou University People's Hospital, 450003 Zhengzhou, China
[23]Department of Radiology, Huaxi MR Research Center (HMRRC), Functional and Molecular Imaging key Laboratory of Sichuan Province, West China Hospital of Sichuan University, 610041 Chengdu, China
[24]Research Unit of Psychoradiology, Chinese Academy of Medical Sciences, 610041 Chengdu, China
[25]Department of Radiology, Hainan General Hospital (Hainan Affiliated Hospital of Hainan Medical University), 570311 Haikou, China
[26]Department of Magnetic Resonance, Lanzhou University Second Hospital, 730030 Lanzhou, China
[27]Gansu Province Clinical Research Center for Functional and Molecular Imaging, 730030 Lanzhou, China
[28]Department of Radiology, Tianjin First Center Hospital, 300192 Tianjin, China
[29]Department of Radiology, The First Affiliated Hospital of Dalian Medical University, 116011 Dalian, China
[30]Department of Radiology, Qilu Hospital of Shandong University, 250012 Jinan, China
[31]Center for MRI Research, Academy for Advanced Interdisciplinary Studies, Peking University, 100871 Beijing, China
[32]Department of Radiology, The First Affiliated Hospital of Wenzhou Medical University, 325000 Wenzhou, China

[33]Department of Radiology, The Affiliated Hospital of Xuzhou Medical University, 221006 Xuzhou, China
[34]Department of Radiology, Beijing Tongren Hospital, Capital Medical University, 100730 Beijing, China
[35]Department of Radiology, Drum Tower Hospital, Medical School of Nanjing University, 210008 Nanjing, China
[36]Division of Life Science and Medicine, University of Science & Technology of China, 230027 Hefei, China
[37]Developmental Population Neuroscience Research Center at IDG/McGovern Institute for Brain Research, Beijing Normal University, 100875 Beijing, China
[38]Institute of Psychology, Chinese Academy of Sciences, 100101 Beijing, China
[39]Key Laboratory of Pollution Processes and Environmental Criteria, Ministry of Education, Tianjin Key Laboratory of Environmental Remediation and Pollution Control, Nankai University, 300350 Tianjin, China
[40]Functional and Molecular Imaging Key Lab of Shaanxi Province & Department of Radiology, Tangdu Hospital, Air Force Medical University, 710038 Xi'an, China
[41]Biomedical Institute, Henan Academy of Sciences, 450199, Zhengzhou, China

[#]These authors contributed equally to this work: Jiayuan Xu, Xiaojun Xu, Zhihan Yan
*Correspondence to:
Chunshui Yu, e-mail: chunshuiyu@tmu.edu.cn
Meiyun Wang, e-mail: mywang@ha.edu.cn
Guangbin Cui, e-mail: cuigbtd@163.com

Supplementary Information

Content

Supplementary Methods

Participants

All participants were recruited by the CHIMGEN study (http://chimgen.tmu.edu.cn/), which collected the genomic, neuroimaging, environmental, and behavioral data from 7,306 healthy Chinese Han participants aged 18-30 years from 32 research centers[1]. The inclusion and exclusion criteria of these CHIMGEN participants are presented in Supplementary Table 1. The recruitment processes, standard operating procedures, and data quality control are given on the website (http://chimgen.tmu.edu.cn/)[1]. The written informed consents were obtained from all participants, and this study was approved by the Medical Research Ethics Committee of Tianjin Medical University General Hospital (IRB2015-092-01) and other institutions. Of the 7,306 CHIMGEN participants, 7,163 had qualified genomic data. Among them, 6,826 were underwent detection of serum concentrations of 21 types of perfluoroalkyl and polyfluoroalkyl substances (PFASs), including 13 types of perfluoroalkyl carboxylic acids (PFCA) and 8 types of perfluorosulfonic acids (PFSA). According to the year of PFAS detection, we divided the participants into the discovery (n = 4,001 to 5,325; three batches detected in 2021) and replication (n = 413 to 1,498; one batch detected in 2022) samples. The chi-square test was used to compare sex difference between the discovery and replication samples, while the two sample t-test was used to compare the differences in other variables.

Serum PFAS concentration detection

Sample collection

Of the 7,163 CHIMGEN participants with qualified genetic data, 6,826 were underwent the concentration detection of PFASs. We collected about 10 ml whole blood from each participant using serum tubes without anticoagulant. Blood was allowed to clot for 20 min and then centrifuged for 15 min at 4000 rpm. Serum was transferred to solvent-rinsed polypropylene vials and stored at -80 °C until PFASs detection. For each participant, we detected the serum concentrations of 21 PFASs, including 13 types of PFCA and 8 types of PFSA (Supplementary Table 2). The pipeline was designed for the detection of serum concentrations of all the 21 PFASs.

Chemicals and reagents

All standard solutions were purchased from Wellington Laboratory (Ontario, Canada). The PFAC-MXB is a mixture of the 21 PFASs under detection, which was used to detect the concentration of each PFAS. The mass-labelled MPFAC-MXA is a mixture of the perfluorooctanoic acid ($^{13}C_2$-PFOA) and perfluorooctane sulfonic acid ($^{13}C_4$-PFOS). As PFOA is a canonical representative of PFCAs and PFOS is a canonical representative of PFSAs, the mass-labelled MPFAC-MXA solution was used in recovery experiments to confirm the accuracy of our PFAS concentration detection. These standard solutions were 2μg/ml with purity ≥ 98%, stored at 4℃ and protected from light. The reagents were mainly purchased from MACKLIN, including

the methanol, ammonium acetate, and acetonitrile with mass spectrometry grade and the sodium bicarbonate, sodium carbonate, and tetrabutylammonium hydrogen-sulfate (TBAHS) with analytical reagent grade. Ultrapure water was used in the whole process of PFAS concentration detection. The 0.22μm filter membrane was purchased from ANPEL Laboratory Technologies Inc. (Shanghai, China).

Sample pretreatment

Serum sample pretreatment for PFAS concentration detection was performed following the procedures described by Hansen et al[2]. Briefly, 200μL of thawed and mixed serum was added into a 15mL polypropylene centrifuge tube at 4℃, followed by the addition of 1mL of 0.5M TBAHS (pH = 10) solution and 2mL of 0.25M sodium carbonate buffer (sodium carbonate and sodium bicarbonate). After mixing on a vortex for 3min, 4mL methyl tert-butyl ether (MTBE) was added, and the mixture was shaken at 250r/min at room temperature for 20min. After centrifugation at 4500r/min for 10min, supernatant was separated and collected in a new polypropylene centrifuge tube. The extraction procedure was repeated two more times. The supernatants were combined, and solvent was dried under a gentle stream of nitrogen (N_2) at 40°C, reconstituted with 200μL methanol, filtered with a 0.22μm organic filter membrane, and then transferred to a polypropylene autosampler vial and stored at -20℃ before analysis.

Instrumental analysis

Serum PFAS concentration was detected using a Waters ACQUITY ultra-performance liquid chromatography (UPLC) system coupled with an Applied Biosystems API 4000 (Sciex, Concord, Ontario, Canada), which was equipped with an electrospray interface operating in negative ion mode. Chromatograms were recorded by multiple reaction monitoring (MRM). The monitoring transitions, declustering potential, and collision energy parameters are shown in Supplementary Table 2. All compounds were separated using an Agilent EC C_{18} column (5μm; 2.1mm × 150mm), which was maintained at 40°C. The 10 μL aliquot of sample was injected and analyzed by the gradient method using 2mM ammonium acetate in Milli Q water (mobile phase A, MPA) and acetonitrile (mobile phase B, MPB). The flow rate was set at 0.3 mL/min, and the program started with 90% MPA and 10% MPB. It ramped to 20% MPB by 1 min, increased to 90% MPB by 4 min, which was held for 2 min, 10% MPB by 6.1 min, held until 8 min, and returned to initial conditions by 8.1 min, with the column equilibrating for an additional 2 min.

Quality control

Upper limit of detection

We estimated the PFAS concentration based on the calibration curve constructed by the PFAC-MXB standard solutions with different concentrations (0.01 ng/mL, 0.02 ng/mL, 0.05 ng/mL, 0.1 ng/mL, 0.2 ng/mL, 0.5 ng/mL, 1 ng/mL, 2 ng/mL, 5 ng/mL, 10 ng/mL and 20 ng/mL). The standard solutions were prepared with methanol and

the calibration curve was constructed for each batch. A standard of PFASs at 1 ng/mL was used for quality control, which was checked after every 10 injections to ensure the stability of PFAS concentration detection. The calibration curve was used for quantification when the quality control standard was within ± 20% of its initial value. If the detected value didn't fall into the standard calibration curve, we would increase the concentration of standard solutions up to 200 ng/mL and repeated the construction of calibration curve to quantify the corresponding PFAS concentration. If the value still didn't fall into the calibration curve, the sample would be diluted within the marked range.

Lower limit of detection

The limits of detection (LOD) and quantification (LOQ) for PFAS concentration were calculated based on a serial dilution of calibrant solutions equivalent to a signal-to-noise ratio of 3 and 10, respectively. PFAS accumulation lower than LOD was defined as NA, while those above LOD but below LOQ would be assigned the corresponding LOQ value divided by the square root of two for the further analysis[3]. Blank extracts were also prepared intermittently to confirm that the detection was free of sample carry-over effects and background interferences.

Spiking recovery and detection rate

The accuracy of the detection method was assessed by spiking recovery experiments using the mass-labelled MPFAC-MXA standards at two concentrations (2 ng/mL and 5 ng/mL). Triplicate recovery experiments were performed with calf serum at each spiked concentration. The recovery rate (RR2 for 2 ng/mL; RR5 for 5 ng/mL) was

252 calculated as the percentage difference between spiked and original concentration of
253 human serum divided by the spiked concentration. Among the 21 PFASs, we
254 successfully detected serum concentrations of 13 PFASs with a detection rate ranging
255 from 77.00% to 99.96% (Supplementary Table 3). The distribution of raw serum
256 PFAS concentration data is shown in Fig. S3.

257 ## *Replicability analysis*

258 To validate the reproducibility of serum PFAS concentration detection, we
259 deliberately included 38 blind duplicate pairs during detection. We calculated Pearson
260 correlation of serum PFAS concentrations between the 38 duplicate pairs, while
261 controlling for age, sex, education, and batch. The robustness of detection was
262 confirmed by the strong correlations of serum PFAS concentrations between the 38
263 technically duplicate pairs (Fig. S2).

264 ## *Data preprocessing*

265 ### *Log2 transformation*

266 The log2 transformation was applied to the raw serum PFAS concentration data with
267 skewed distribution to make the data with approximate normal distribution (Fig. S3).

268 ### *Batch effect correction*

269 As serum PFAS concentrations were detected in four batches, we performed principal
270 component analysis (PCA) to test the batch effect of PFAS concentration detection,
271 and found potential batch effect (Figs. S4 and S6). Then, we conducted analysis of

variance (ANOVA) for PFAS concentrations obtained from these batches and found significant differences (Fig. S4) among the four batches. Thus, ComBat function implemented in *sva* R package[4] was utilized to harmonize PFAS concentrations across batches, which can remove between-batch variation and preserve biological variability. We repeated PCA and ANOVA for the batch-corrected PFAS accumulation data, and did not find any significant batch effect (Fig. S6).

Gene expression data processing

RNA-seq quantification

We quantified the transcription at gene expression levels using a customized Nextflow workflow[5]. Before quantification, we used Trim Galore v.0.5.0 to remove sequencing adapters (8 bp at the beginning and 7 bp at the end of each fastq read) from the fastq files. HISAT2 v.2.1.0[6] was used to align the reads to the GRCh38 reference genome (Homo_sapiens.GRCh38.dna.primary assembly.fa file, downloaded from Ensembl). We counted the number of reads overlapping with genes in GENCODE v.30[7] reference transcriptome annotations using featureCounts v.1.6.4[8]. All quantification methods were implemented in the eQTL-Catalogue/rnaseq workflow and are free available from GitHub (https://github.com/eQTL-Catalogue/rnaseq).

RNA-seq quality control

To exclude contaminated RNA samples, we checked the sex-specific gene expression data and sample identity[9]. We extracted all protein-coding genes from Y chromosome and the *XIST* gene (ENSG00000229807) from X chromosome, which were normalized into transcripts per million (TPM) using log2 transformation. We then

calculated the mean expression of all genes on the Y chromosome. Finally, we plotted a map to show the relationship between the *XIST* expression (x axis) and mean gene expression on the Y chromosome (y axis) (Fig.S8). We found one self-reported male participant with high *XIST* expression but low gene expression on Y, indicating sex mismatching or RNA sample contamination. This participant was excluded from the subsequent analyses. All quality control processes were implemented in the eQTL-Catalogue/rnaseq workflow obtained from GitHub (https://github.com/eQTL-Catalogue/qcnorm).

RNA-seq normalization

After downloading gene GC content estimates from Ensembl biomaRt, we normalized the gene-level read counts using the conditional quantile normalization (cqn) R package v.1.30.0[10] with gene GC content as a covariate. We excluded lowly expressed genes with TPM expression < 1.00 in 95% samples. The normalization was implemented in the eQTL-Catalogue/rnaseq workflow (https://github.com/eQTL-Catalogue/qcnorm). Finally, we obtained the qualified normalized expression values of 20,830 genes in 573 participants (Supplementary Table 12).

MRI data acquisition and preprocessing

Structural MRI data preprocessing

Among the 6,826 participants with qualified genetic and PFAS concentration data, up to 6,741 participants with qualified structural MRI data. The data were preprocessed

using FreeSurfer v7.0 (http://surfer.nmr.mgh.harvard). After separating the brain tissue from the non-brain tissues using automated skull-stripping, intensity non-uniformity due to variation in reception coil sensitivity and gradient-driven eddy currents were corrected. Based on intensity and neighbor constraints, the skull-stripped and intensity-normalized images were segmented to generate the boundary between gray matter (GM) and white matter (WM). A two-dimensional tessellated mesh was constructed based on the GM-WM boundary to generate the WM surface in each cerebral hemisphere. The WM surface was extended outwards by tracking the GM intensity gradient to generate the pial surface. Topology correction was then performed to repair topological defects. CT and CSA were calculated based on the pial and WM surfaces. Individual surfaces were then inflated into a spherical space and registered to a spherical atlas in MNI152 space (the fsaverage atlas). To reduce noise and the misalignment during the surface-based transformation to the average template, the surface-based metrics were smoothed with a Gaussian kernel of 20-mm width. The mean cortical thickness (MCT) and total surface area (TSA) of each participant were calculated and used as covariates in the CT and SA analyses, respectively. Finally, 5,359 to 6,741 participants with qualified PFAS accumulation and surface data were included in the vertex-wise association analyses.

Diffusion MRI data preprocessing

The diffusion MRI data were preprocessed using the FMRIB's Software Library (FSL v5.0.10) toolbox (www.fmrib.ox.ac.uk/fsl). The non-brain tissues of b = 0 images

were removed by the brain extraction tool. An “EDDY_OPENMP” program was utilized to evaluate and repair the image displacement and signal dropout caused by head motion and image distortion caused by eddy current. The linear least square algorithm was used to estimate diffusion tensor and calculate diffusion metrics (FA and MD) using the DTIFIT program. Individual b = 0 images were aligned to structural images using the Boundary-Based Registration (BBR) algorithm[70], and then the BBR parameters were concatenated with DARTEL deformation field generated in normalization of structural images. The merged deformation field was used to register individual FA and MD maps to MNI space using the tract-based spatial statistics (TBSS) pipeline and resampled into a cubic voxel of 2mm. After co-registering individual FA images into MNI space using the merged deformation field, a mean FA image was created and a mean FA skeleton of the white matter was generated using the center-of-gravity method. Individual’s aligned FA images were projected onto the mean FA skeleton by filling the skeleton with FA values from the nearest relevant tract center. The process was achieved by searching perpendicular to the local skeleton structure for maximum value. The obtained projection parameters were applied to the MD map of the participant to generate voxel-wise MD images on the white matter skeleton. Finally, 5,357 to 6,739 participants with qualified PFAS and skeletonized FA and MD maps were included in the voxel-wise TBSS analyses.

Behavioral assessments

Mental health assessments

The Beck depression inventory (BDI-II)[11] was used to assess depressive symptoms; the state-trait anxiety inventory (STAI)[12] was used to assess state (SA) and trait anxiety (TA); and the positive and negative affect schedule (PANAS)[13] was used to evaluate positive (PANAS-P) and negative (PANAS-N) emotions and moods.

Personality assessments

The NEO big five inventory[14] and the tridimensional personality questionnaire (TPQ)[15] were used to measure eight personality traits. NEO traits included agreeableness (NEO-A), conscientiousness (NEO-C), extraversion (NEO-E), neuroticism (NEO-N), and openness (NEO-O), while TPQ traits included harm avoidance (TPQ-HA), novelty seeking (TPQ-NS), and reward dependence (TPQ-RD).

Cognitive assessments

Verbal learning and memory. The second edition of California Verbal Learning Test (CVLT-II) was used to assess verbal learning and memory[16]. The word list A included 16 words of four semantic categories (furniture, vegetable, vehicle, and animal) and the interference list B also included 16 words of four categories (vegetable, animal, musical instrument, and house part name; the former two from the word list A). There were five trials for the word list A and one trial for the word list B, and the words were randomly presented irrespective of semantic categories. In each trial, the experimenter read aloud the word list in one word per second and then the participant was asked to recall the words as many as possible. After the five trials for the word

list A, the participant was asked to learn and recall the word list B once. After the trial for the word list B, the participant was asked to recall the word list A immediately (short delay) and 20 minutes later (long delay). The participant should recall the words in no order in free recall and should categorize the words into four categories in cued recall. The number of correct words in the five trials for the word list A was used to assess immediate free recall (CVLT-IFR). The numbers of correct words in the four recall tasks were used to assess the short delayed free recall (CVLT-SDFR), short delayed cued recall (CVLT-SDCR), long delayed free recall (CVLT-LDFR), and long delayed cued recall (CVLT-LDCR).

Working memory. The letter N-back test was applied to assess working memory[17]. In 1-back task, the participant was asked to judge if the current stimulus matched the previous one in the sequence of stimuli. In 3-back task, the participant was asked to judge whether the current stimulus matched the one 3-steps earlier. Both tasks included 60 trials and each stimulus was presented for 200ms with an interval of 1800ms. E-Prime 2.0 was used to present stimuli and collect results. The correct rate (CR) of 1-back task was used to assess compliance and participants with CR < 75% were excluded. The CR of 3-back task (N-BACK-CR) was used to assess working memory.

Visuospatial memory. The Rey-Osterrieth complex figure test (ROCFT) was used to assess visuospatial ability[18]. Each participant was asked to copy and recall a complex line graph at three different time points: copying the graph at the beginning (copying); redrawing the graph from memory immediately (immediate recall); and reproducing the graph from memory 25 minutes later (delayed recall). A 36-point scoring system was used to assess the correct rates of the three tasks based on the scoring guideline for each element. As the scoring system is susceptible to inter-rater

variability, all ROCFT assessments were completed by a trained and fixed group of raters to achieve consistent results. Finally, the scores of immediate (RO-IR) and delayed recall (RO-DR) were used to assess visuospatial memory.

Information processing speed. The symbols digit modality test (SDMT) was used to evaluate information processing speed[19]. The test consisted of single digits paired with abstract symbols. The keys contained nine abstract symbols, corresponding to nine numbers. Each participant was asked to see the keys and to write the corresponding numbers as fast as possible within 90s. The number of correct responses (SDMT-COR) was used to assess the information processing ability.

Social cognition. A ball tossing game with a 2 × 2 factorial design was applied to assess perspective taking (first-person and third-person perspective) and agency (active and passive)[20]. Each participant was asked to perform active and passive tasks from two different perspectives. From the third-person perspective (3PP), three virtual characters (red, green, and blue) appeared on the screen to perform a ball tossing game. The participant performed the active and passive tasks from the blue character's perspective. In the active task, the participant (blue character) was instructed to throw the ball to the red character when he/she was in possession of the ball. The participant should judge the red character's position from the blue character's perspective by pressing the key "F = left" or "J = right". In the passive task, one of the red or green character was in possession of the ball, and the participant should judge the ball's position from the blue character's perspective with a button press "F = left" or "J = right". The first-person perspective (1PP) is the

forward vision of the blue character. Only one hand of the blue character was displayed on the screen. The participant was then asked to perform the active and passive tasks. The whole task includes four blocks in the order of 1PP, 3PP, 3PP and 1PP. Each block contains 18 trials including 6 active and 12 passive tasks. The location of the blue character, the character in possession of the ball, and the relative position of the red character are presented pseudo-randomly. After two practices, the participant conducted the formal test by responding as fast and accurately as possible. E-Prime 2.0 was also used to present stimuli and collect results. We recorded the active (1PP-ACT-ACC and 3PP-ACT-ACC) and passive (1PP-PAS-ACC and 3PP-PAS-ACC) accuracy in the 1PP and 3PP tests. The accuracy in perspective taking (PT-ACC) was defined as (3PP-ACT-ACC + 3PP-PAS-ACC) - (1PP-ACT-ACC + 1PP-PAS-ACC), and the accuracy in agency (AGE-ACC) was defined as (3PP-PAS-ACC + 1PP-PAS-ACC) - (3PP-ACT-ACC+1PP-ACT-ACC).

Executive control. The go/no-go test was used to assess executive control ability. In “go” condition, the current letter is different from the previous one and the participant should respond quickly by pressing the button. In “no-go” condition, the current letter was the same as the previous one (10% trials) and the participant should not press the button. If one pressed the button, it would be counted as an error. The test included two blocks and each block included 21 go-trials and 189 no-go-trials. The participant was instructed to respond as fast and accurately as possible. E-Prime 2.0 software was used to present stimuli and collect results. The correct rate in no-go-trials (NO-GO-CR) was used to assess executive control ability.

Confounding covariates

Throughout analyses, we controlled for age at data acquisition, genetic-determined sex, years of education, living city at recruitment, and batches for serum PFAS detection. In the sensitivity analysis, we additionally controlled for lifetime socioeconomic status (SES), occupation, breastfeeding, urbanicity score, air pollution, and serum accumulation of four heavy metals.

Lifetime SES assessment. For each participant, SES was assessed by the following items, including parental education (1 = primary school or below; 2 = middle school; 3 = high or technical school; 4 = junior college; 5 = bachelor; 6 = master or doctor), parental occupations (1 = unemployed or day laborer; 2 = manual worker or self-employed; 3 = equipment operator; 4 = production personnel; 5 = business or service staff; 6 = civil servant or company employee; 7 = professional and technical personnel; 8 = manager), family unemployment pressure (1 = often, 2 = occasional, 3 = never), family financial difficulty (1 = often, 2 = occasional, 3 = never), family financial crisis (1 = often, 2 = occasional, 3 = never), dwelling space inadequacy (1 = crowd, 2 = moderate, 3 = spacious), and neighborhood indifference (1 = poor, 2 = moderate, 3 = harmonious). Except for parental education, all SES indicators were assessed for three age windows (< 10 years, 11-20 years or 11-present age, and > 20 years). All items were categorical variables, and higher scores represent higher SES levels. Items were *z*-scored and then summed up as the final SES score of each participant. Lifetime SES was calculated by averaging SES scores of the three age windows.

Occupation. For each participant, their own occupation was also considered as a covariate (1 = unemployed or day laborer; 2 = manual worker or self-employed; 3 = equipment operator; 4 = production personnel; 5 = business or service staff; 6 = civil servant or company employee; 7 = professional and technical personnel; 8 = manager).

Breastfeeding. As PFAS levels were associated with breastfeed[21], breastfeed status was also included as a covariate (1 = breastfeed; 2 = no breastfeed; 3 = unknow).

Urbanicity score. According to population density, the living place was classified into three categories: rural area = 1, town = 2, and city = 3. Each participant was asked to report the category of each place they had lived and the duration of residence in each location before age 18. An urbanicity score was calculated by multiplying the category value of each place by the number of years lived there between birth and age eighteen, and then summing these products[22]. The urbanicity score ranged from 18 to 54.

Air pollution. Each participant was asked to recall residential coordinates of the years from birth to recruitment. If the participant moved in a year, the coordinates where they lived for the longest duration was defined as the residential coordinate of that year. The annual PM2.5 data were provided by a prior study[23], based on which we extracted annual PM2.5 data for each participant from birth to recruitment. The average PM2.5 values of the annual data for the available years were used to represent air pollution exposure.

Heavy metals. We also included four heavy metals with known neurotoxicity, including chromium, nickel, arsenic and lead. Serum heavy metal concentration was detected by inductively coupled plasma mass spectrometry (ICP-MS) coupled with a NexION 300D (PerkinElmer Inc., USA).

Genome-wide associations with serum PFAS accumulation

We constructed a sample-specific LD reference using the imputed genotype data from the 6,826 CHIMGEN participants. With the LD reference, we conducted PLINK clumping to identify independent genetic variants associated with PFAS accumulation from all variants with significant associations ($P < 3.85 \times 10^{-9}$) with the following steps: (a) all variants with significant associations were used to construct a list of candidate variants; (b) the most significant variant was defined as the first lead variant and other variants within 500 kb from and in LD ($r^2 > 0.6$) with the lead variant were clumped; (c) the remaining variants formed a new list of candidate variants and then the step (b) was repeated; and (d) the iterative process stopped until the list was empty. The remaining lead variants were defined as the independent variants. Then, we identified the independent loci associated with serum PFAS accumulation by the following steps: (a) creating loci for all independent genetic variants by adding 500 kb to both sides of each variant; (b) merging overlapping loci; (c) merging loci if an independent variant of one given locus was in LD ($r^2 > 0.6$) with any independent variant of other loci. The remaining loci were defined as independent loci.

SMR and HEIDI analyses

We identified the causal associations between gene expression and PFAS accumulation using the summary data-based Mendelian randomization (SMR)[24]. In the SMR tests, we defined phenotype (PFAS accumulation) as y, exposure (gene expression) as x, instrumental variables (eSNPs) as z, the effect of z on x as b_{zx}, the effect of z on y as b_{zy}, and the effect size of x on y as $b_{xy}=b_{zy}/b_{zx}$. b_{xy} was interpreted as the effect of x on y free of non-genetic confounders. Here, SMR was used to test the causal effect (b_{xy}) of gene expression (x) on serum PFAS levels (y) using the SNPs as instrumental variables ($P_c < 0.05$, Bonferroni corrected for the number of genes tested).

An observed association in an SMR test could be due to any one of the following three relationships: causality (the effect of a SNP on PFAS accumulation is mediated by gene expression); pleiotropy (a SNP has direct effects on both PFAS accumulation and gene expression); and linkage (a SNP is in LD with two distinct causal variants, one impacting gene expression and the other impacting PFAS accumulation). Thus, a heterogeneity in dependent instruments (HEIDI) test was applied to multiple SNPs in a *cis*-eQTL region (± 1Mb from the center of the gene) to further exclude the linkage associations of less biological interest. Under the hypothesis of pleiotropy or causality, where gene expression and PFAS accumulation share the same causal variant, the b_{xy} values of any SNPs in LD with the causal variant are identical. Therefore, testing against the null hypothesis that there is a single causal variant is equivalent to testing whether there is heterogeneity in the b_{xy} values estimated for the SNPs in the

cis-eQTL region. For gene expression that passed the significance threshold for the SMR test, we used the HEIDI method to test the heterogeneity in the b_{xy} values estimated for multiple SNPs in the *cis*-eQTL region. A HEIDI $P > 0.05$ was used since it is conservative for discovery by retaining fewer genes than correcting for multiple testing.

Neurotoxicity of serum PFAS accumulation

Serum PFAS accumulation and brain structural imaging measures

Addressing Mendelian randomization assumptions

To ensure the robustness of one-sample MR analyses, we validated the selected IVs against the three key MR assumptions:

(1) Relevance assumption: According to the relevance assumption, IVs should be strongly associated with the exposure. An *F*-statistic >10 in the linear relationship between IVs and exposure is accepted as an indicator of a strong instrument[25]. As shown in Supplementary Table 20, the identified four IVs were significantly associated with PFHpA accumulation, yielding an *F*-statistic of 24.81 with the formula (1) and (2), which exceeds the threshold of 10[25]. This indicates that the relevance assumption of MR is validated.

$$R^2 = \frac{2 \times (\beta^2)}{2 \times (\beta^2) + (se^2) \times 2 \times N}$$

$$F = \frac{R^2\,(N - K - 1)}{K(1 - R^2)}$$

(2) Absence of horizontal pleiotropy assumption: We employed the MR

pleiotropy residual sum and outlier (MR-PRESSO) method[26] to test for horizontal pleiotropy ($P < 0.05$ in MR-PRESSO global test). The results suggested the absence of horizontal pleiotropy while testing the causal effect of PFHpA accumulation on the right FMGS-CSA ($P = 0.40$) and anxiety ($P = 0.11$).

(3) Independence assumption: According to previous studies[27,28,29], we calculated *E*-value to validate the independent assumption that the IVs are not associated with any confounders between exposure and outcome. E-value estimates the minimum strength of unmeasured confounding necessary to negate the observed effects. Based on the scaled outcome, we calculated odds ratio (OR) and *E*-value for each association using the same covariates. We found OR = 0.70 (95% CI = 0.55-0.90) and *E*-value = 2.20 (95% CI = 1.45-3.01) for the effect of PFHpA on the right FMGS-CSA, and OR = 1.29 (95% CI = 1.00-1.65) and *E*-value = 1.89 (95% CI = 1.01-2.70) for the effect of PFHpA on anxiety. The higher *E*-value relative to OR indicates that the observed effects were less likely to be influenced by unmeasured confounders[27,28,29].

Supplementary Figures

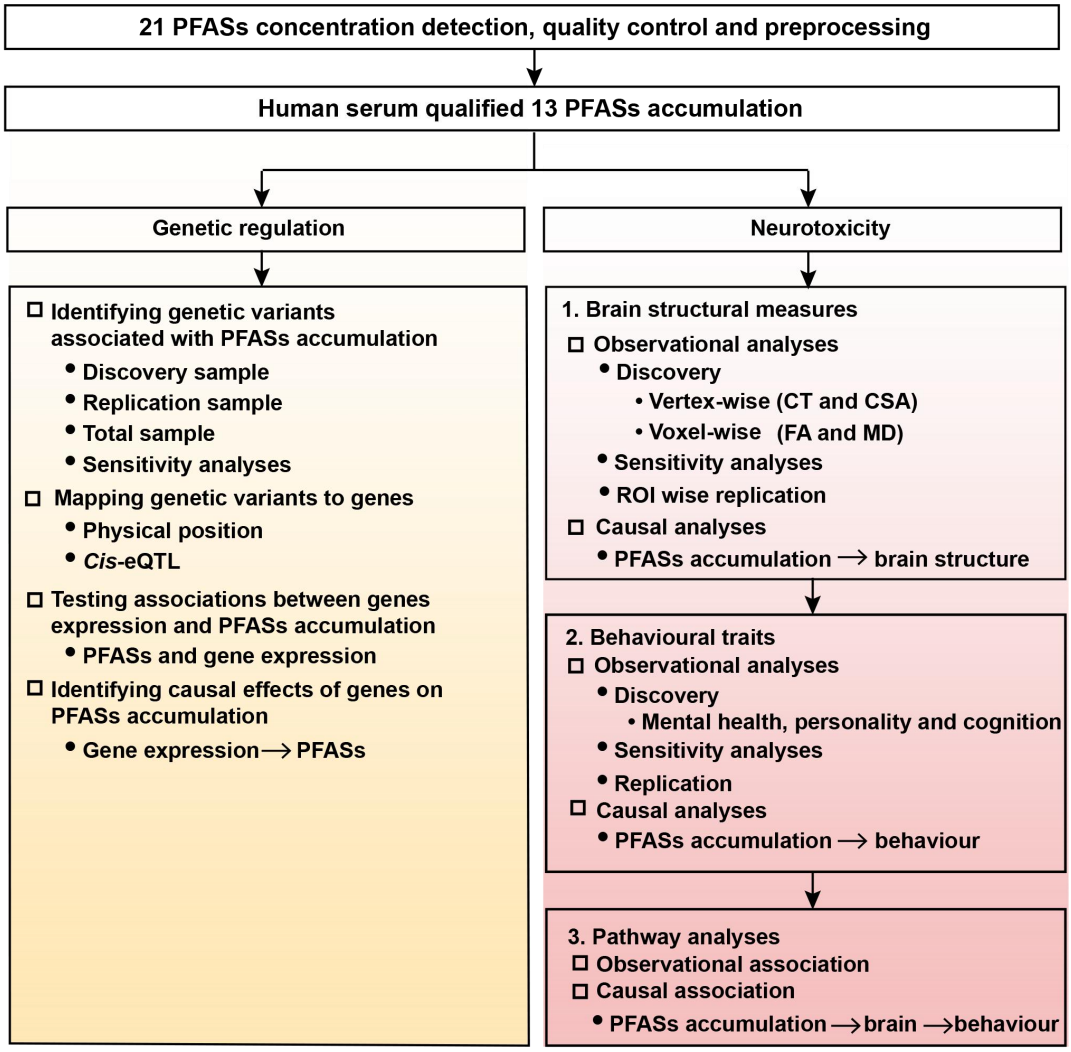

Supplementary Figure 1 | Schematic summary of the study. Abbreviations: *cis-eQTL, cis-expression quantitative trait loci; CSA, cortical surface area; CT, cortical thickness; FA, fractional anisotropy; MD, mean diffusivity; PFASs, perfluoroalkyl and polyfluoroalkyl substances; ROI, region of interest.*

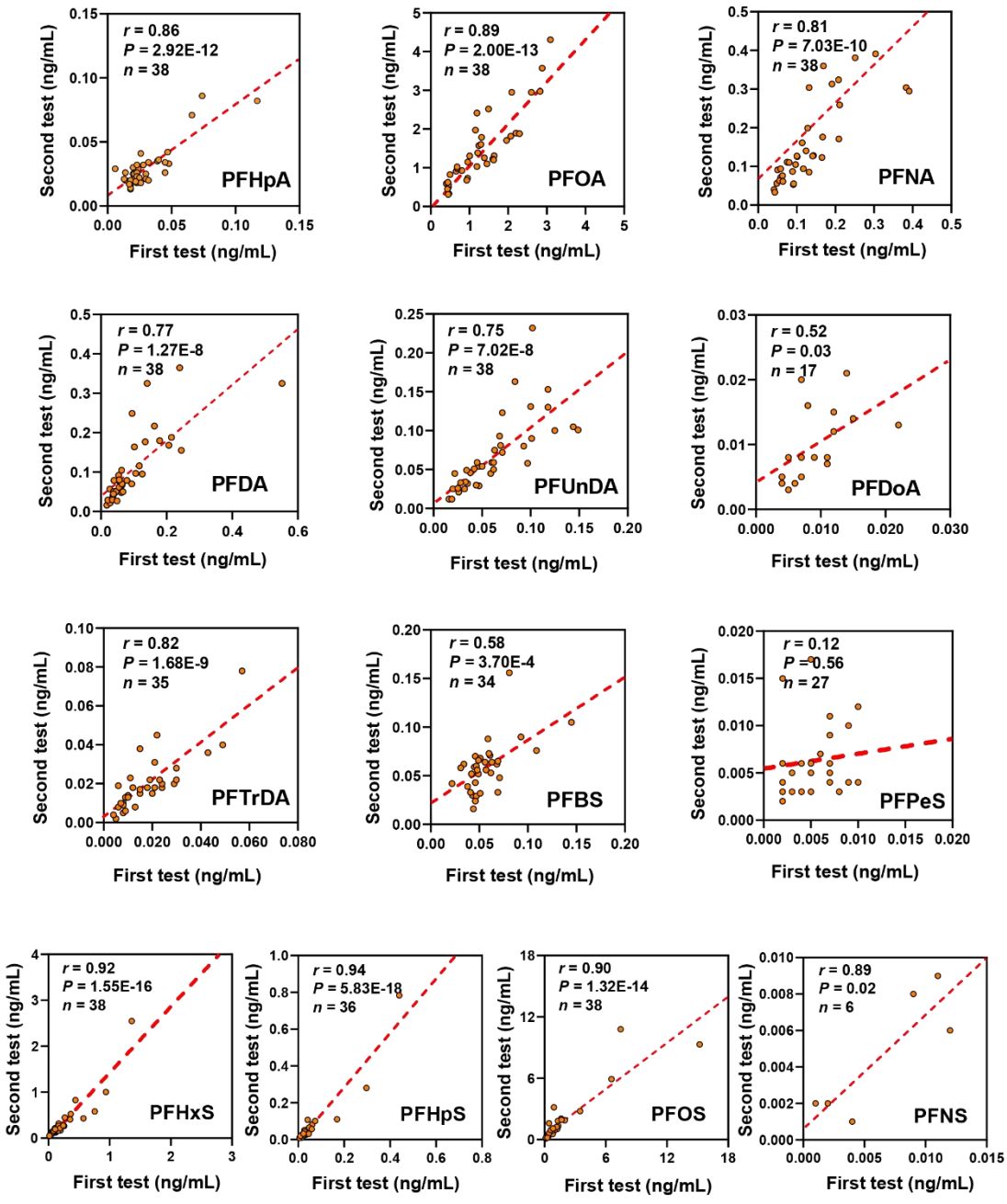

573

574 ***Supplementary Figure 2 | Correlations of PFAS concentrations between technically***

575 ***duplicate pairs.*** *Abbreviations of 13 PFASs are shown in Supplementary Table 2.*

576

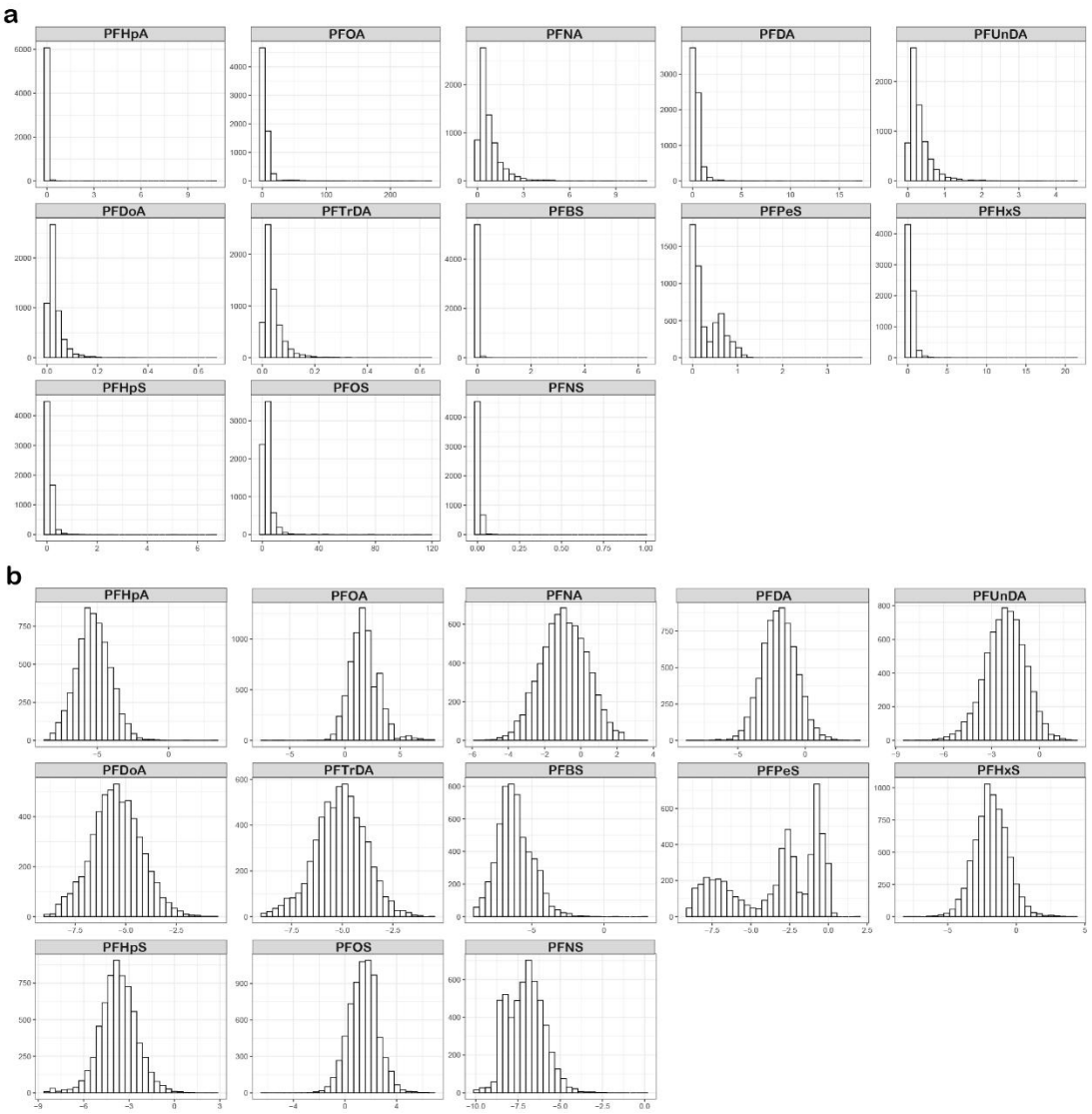

Supplementary Figure 3 | Raw (a) and log2 transformed (b) data distribution of serum PFAS concentrations in the total sample. *Abbreviations of 13 PFASs are shown in Supplementary Table 2.*

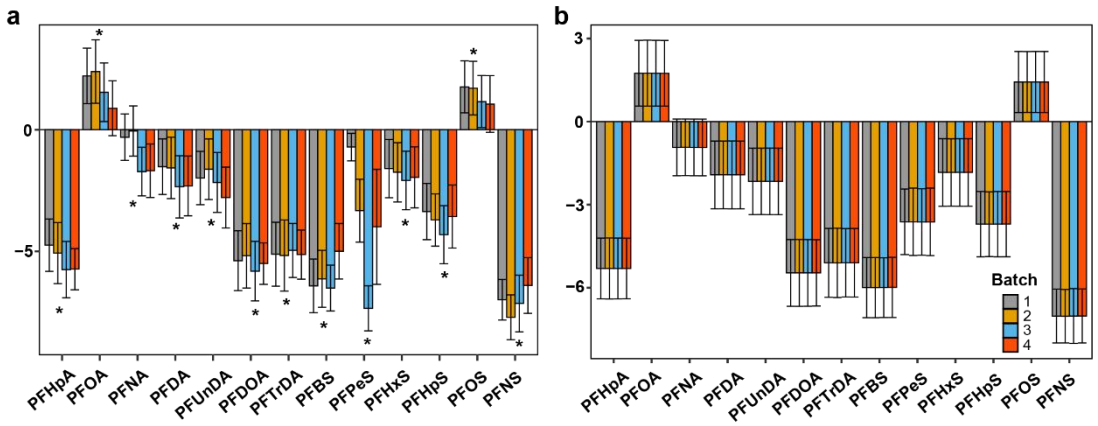

582

583 ***Supplementary Figure 4 | Batch effects before and after correction.*** *The batch*
584 *effects in PFAS concentration detection before (a) and after (b) ComBat*
585 *harmonization. Bar plots show the intergroup differences in PFAS concentrations*
586 *among the four batches before (a) and after (b) batch effect correction. Abbreviations*
587 *of 13 PFASs are shown in Supplementary Table 2.*

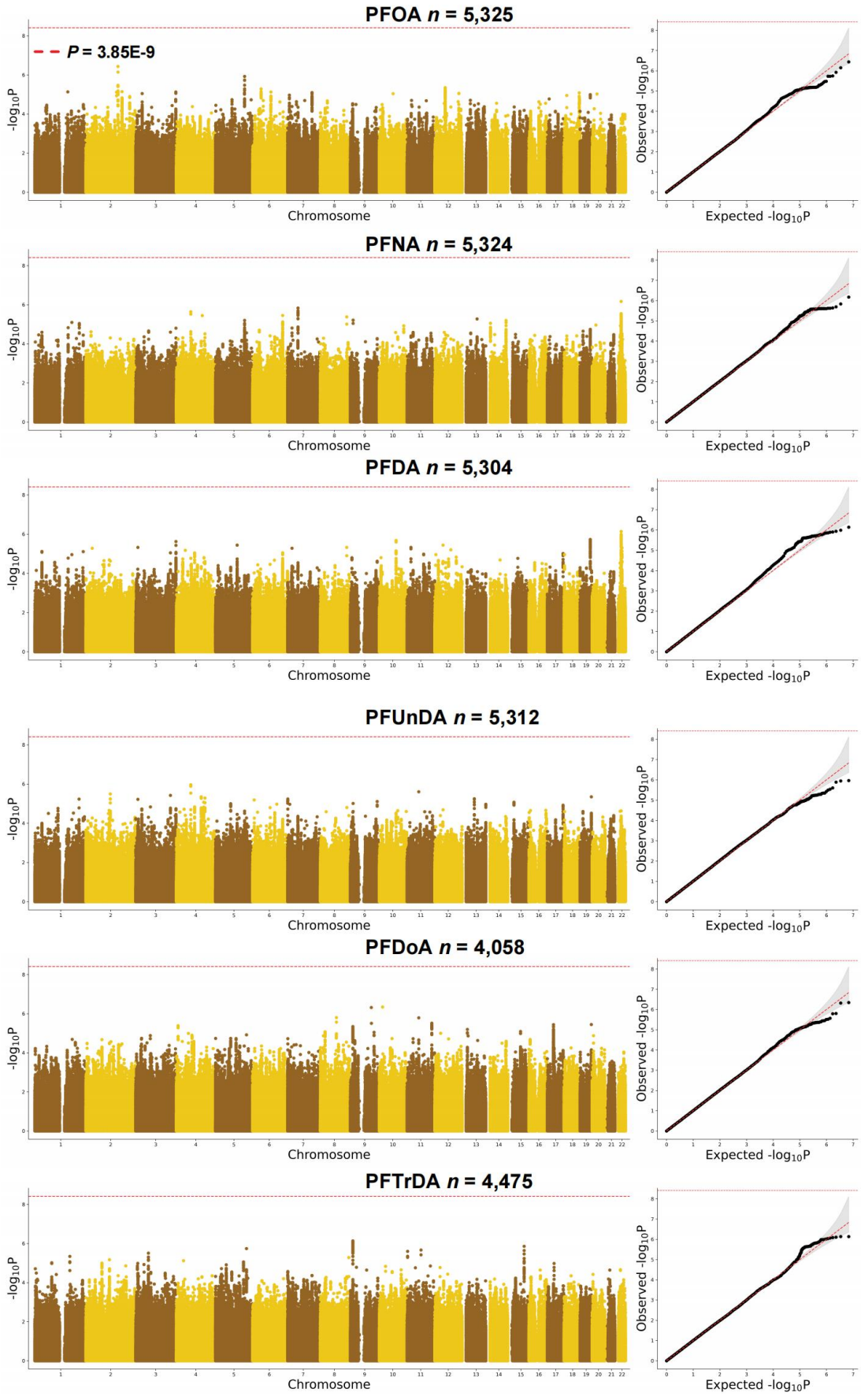
PFOA n = 5,325
P = 3.85E-9
PFNA n = 5,324
PFDA n = 5,304
PFUnDA n = 5,312
PFDoA n = 4,058
PFTrDA n = 4,475
-log10P
Chromosome
Observed -log10P
Expected -log10P

588

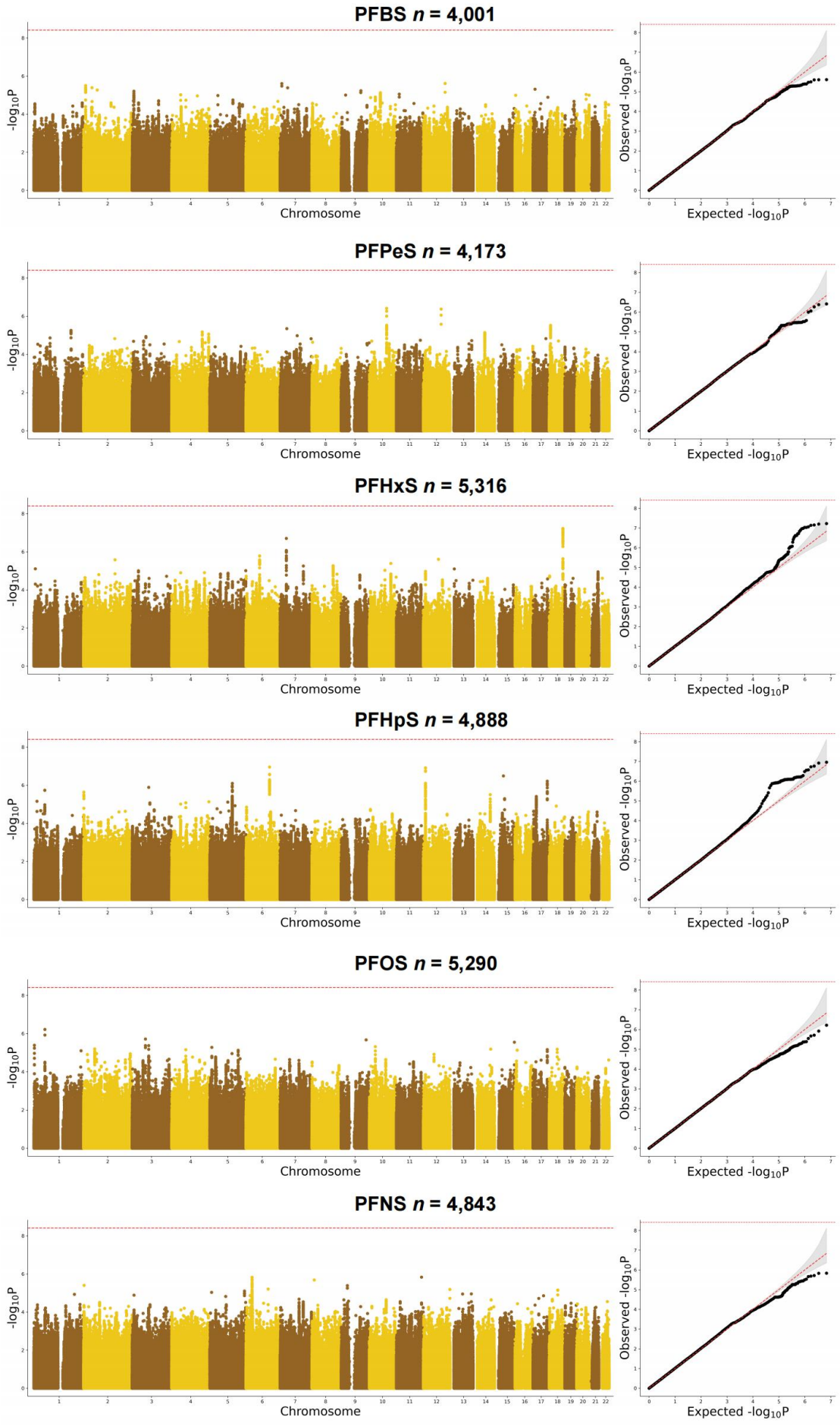
PFBS n = 4,001
PFPeS n = 4,173
PFHxS n = 5,316
PFHpS n = 4,888
PFOS n = 5,290
PFNS n = 4,843
-log10P
Chromosome
Observed -log10P
Expected -log10P

589

Supplementary Figure 5 | Genome-wide associations with serum accumulation of 12 PFASs in the discovery sample. *Manhattan (left) and quantile–quantile plots (right) show the study-wide significant associations (red dashed line, $P < 3.85 \times 10^{-9}$) with serum accumulation of 12 PFASs in the discovery sample. Abbreviations of 12 PFASs are shown in Supplementary Table 2.*

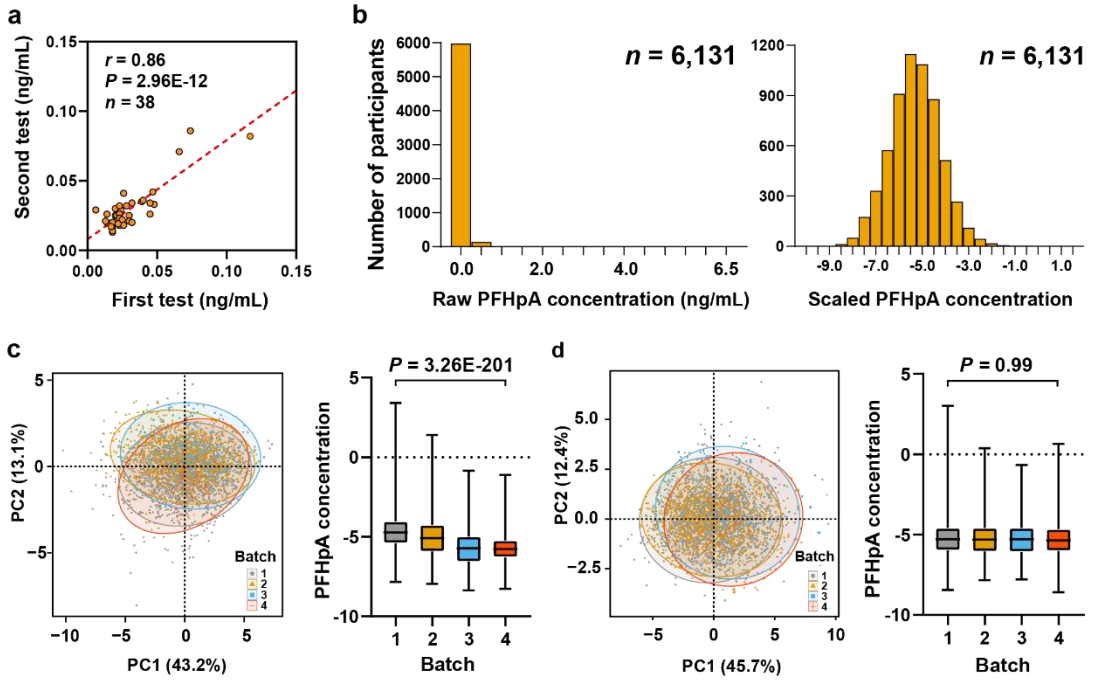

Supplementary Figure 6 | An example of quality control and preprocessing of serum PFAS concentration data. *We use PFHpA as an example to show quality control and preprocessing of serum PFAS data.* ***a****, Scatter plot shows a strong correlation (Pearson correlation, r = 0.86, P = 2.96 × 10^{-12}) in serum PFHpA concentrations between 38 technically duplicate pairs.* ***b****, Histograms show raw (left panel) and log2-transformed (right panel) data distribution of PFHpA concentrations in the 6,131 participants.* ***c-d****, The batch effects in PFHpA concentration detection before (**c**) and after (**d**) ComBat harmonization. In the left panels, scatter plots from principal component analyses show the data distribution of PFHpA concentrations detected by four batches before (**c**) and after (**d**) batch effect correction. In the right panels, bar plots show the intergroup differences in PFHpA concentrations among the four batches before (F = 334.60, P = 3.26 × 10^{-201}) and after (F = 0.0002, P = 0.99) batch effect correction.* ***Abbreviations:*** *PC, principal component; PFHpA, Perfluoroheptanoic acid.*

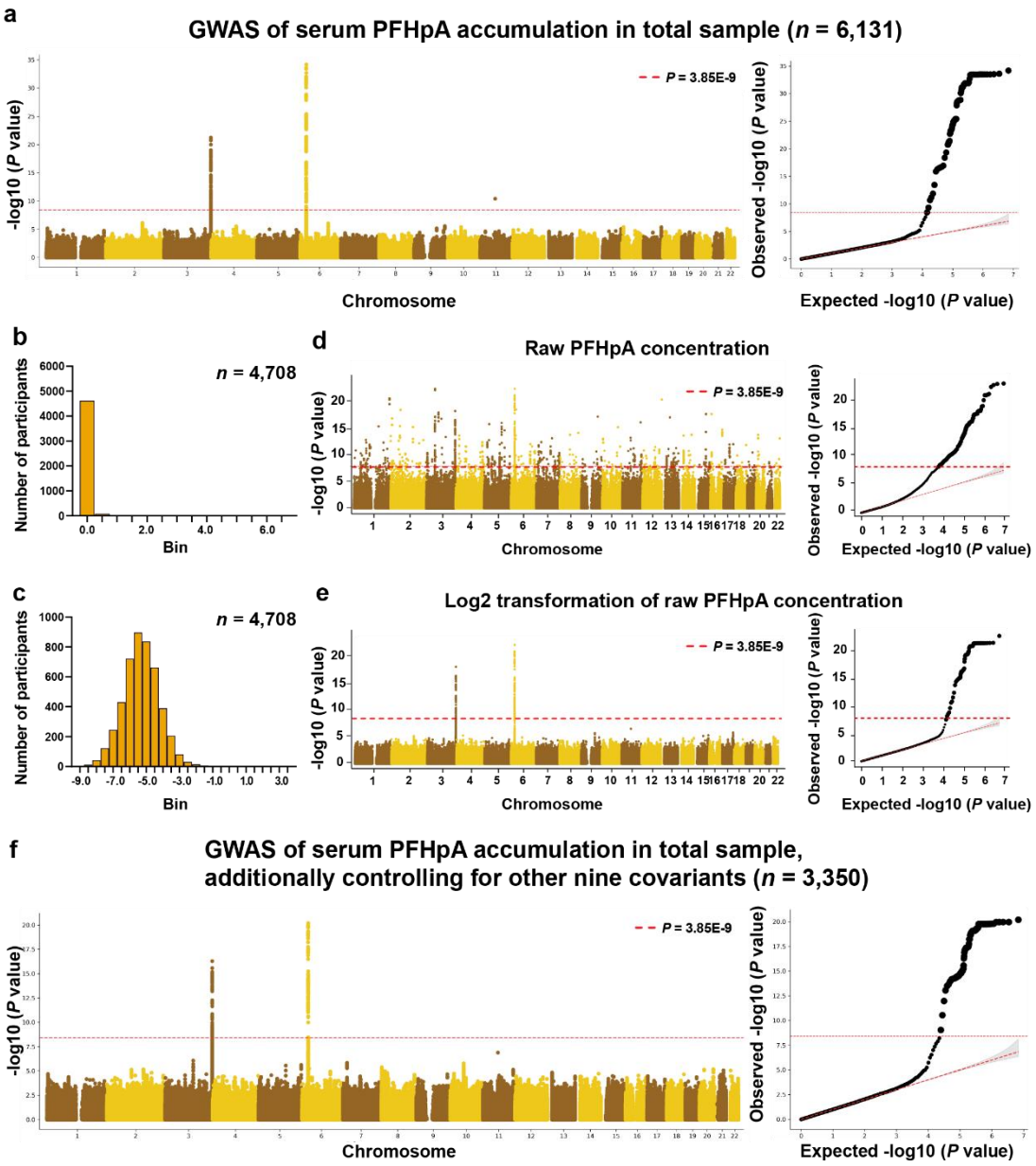

613

614 ***Supplementary Figure 7 | Sensitivity analyses for genome-wide associations with***
615 ***serum PFHpA accumulation.*** ***a****, Manhattan (left) and quantile–quantile plot (right)*
616 *show the genome-wide significant associations with serum PFHpA concentration in*
617 *6,131 participants, controlling for age, sex, education, living city at recruitment,*
618 *PFAS detection batches, and the first ten genetic principal components.* ***b-c****,*
619 *Histograms show raw (b) and log2-transformed (c) data distribution of PFHpA*
620 *concentrations in the discovery sample (n = 4,708).* ***d-e****, Manhattan (left panel) and*
621 *quantile-quantile (right panel) plots show the genome-wide associations with raw (d)*
622 *and log2-transformed (e) PFHpA accumulation in the discovery sample (n = 4,708).* ***f****,*
623 *Manhattan (left panel) and quantile-quantile (right panel) plots show the*

genome-wide associations with serum PFHpA accumulation in a subset of 3,350 participants, additionally controlling for lifetime socioeconomic status, occupation, breastfeeding, urbanicity, air pollution (PM2.5), and serum accumulation of four heavy metals (chromium, nickel, arsenic, and lead). The red dashed line shows study-wide significance threshold of $P = 3.85 \times 10^{-9}$. ***Abbreviations****: GWAS, genome-wide association study; PFHpA, perfluoroheptanoic acid.*

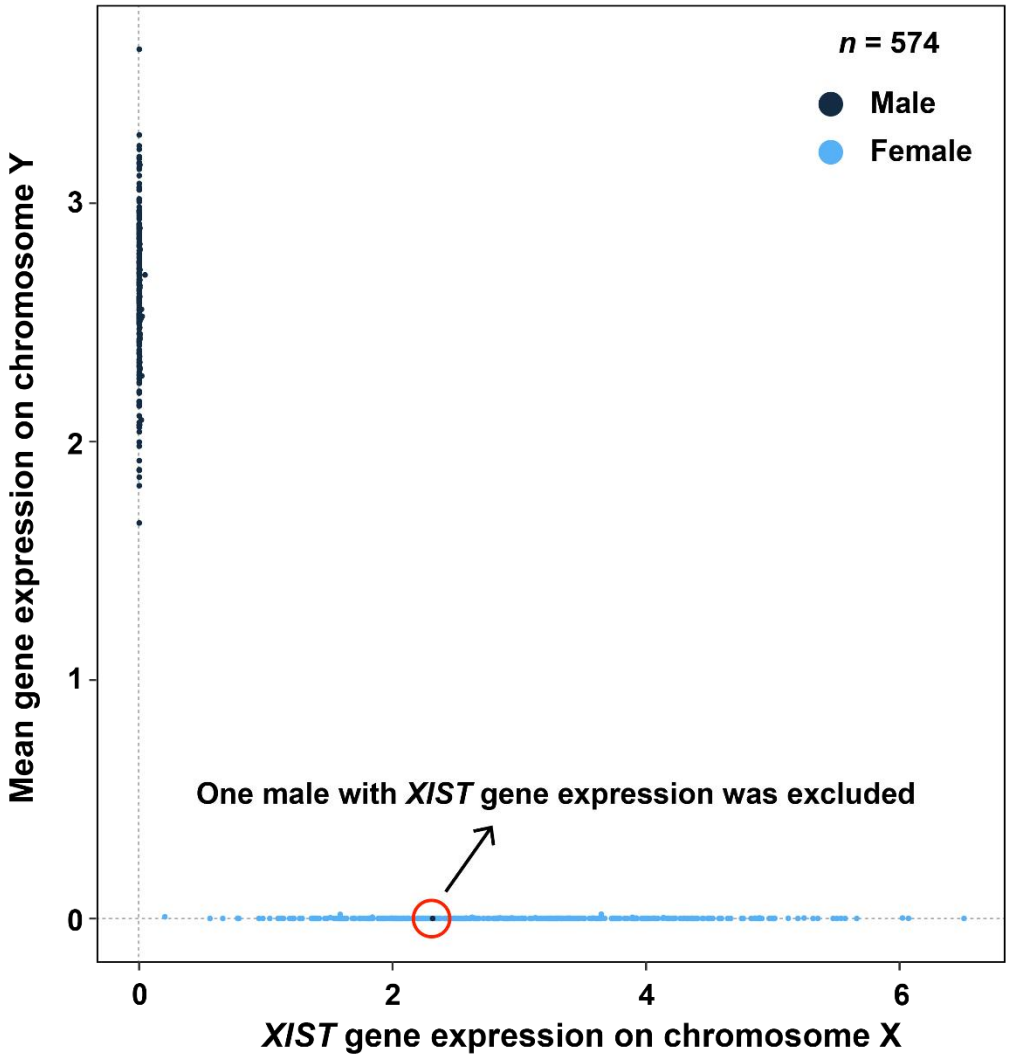

631

632 ***Supplementary Figure 8 | XIST gene expression on chromosome X against the***
633 ***mean expression of genes on chromosome Y in the 574 participants with RNA***
634 ***sequencing data.*** *This is a quality control procedure to identify and exclude*
635 *participants with sex mismatching or RNA sample contamination. One reported male*
636 *participant shows high XIST gene expression on chromosome X but very low gene*
637 *expression on chromosome Y, which is excluded from the sequent analyses.*
638 ***Abbreviation:*** *XIST, X-inactive specific transcript.*

639

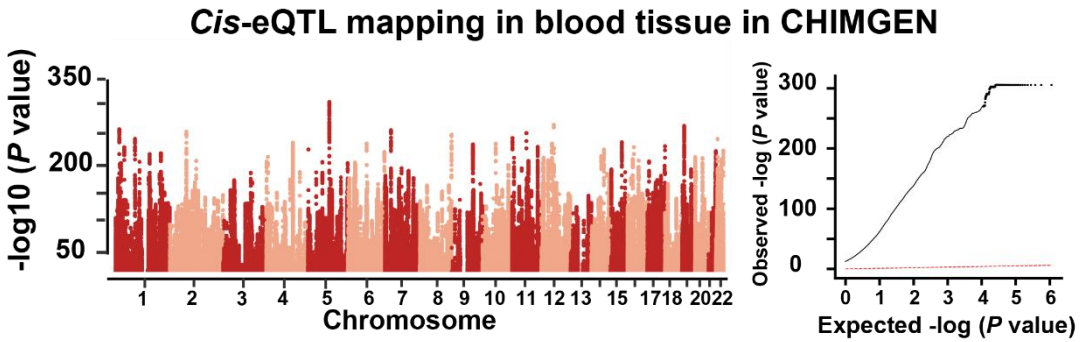

640 ***Supplementary Figure 9 | Cis-eQTL mapping in a subsample.*** *Manhattan (left panel)*
641 *and quantile-quantile plots (right panel) show statistically significant cis-eQTL*
642 *mapping in blood sample of 573 participants at* $P < 5 \times 10^{-8}$. ***Abbreviation:*** *cis-eQTL,*
643 *cis-expression quantitative trait loci.*

644

References

(1) Xu, Q.; Guo, L.; Cheng, J.; Wang, M.; Geng, Z.; Zhu, W.; Zhang, B.; Liao, W.; Qiu, S.; Zhang, H.; et al. CHIMGEN: a Chinese imaging genetics cohort to enhance cross-ethnic and cross-geographic brain research. *Mol Psychiatry* **2020**, *25* (3), 517-529. DOI: 10.1038/s41380-019-0627-6 From NLM.

(2) Hansen, K. J.; Clemen, L. A.; Ellefson, M. E.; Johnson, H. O. Compound-Specific, Quantitative Characterization of Organic Fluorochemicals in Biological Matrices. *Environmental Science & Technology* **2001**, *35* (4), 766-770. DOI: 10.1021/es001489z.

(3) Forthun, I. H.; Roelants, M.; Haug, L. S.; Knutsen, H. K.; Schell, L. M.; Jugessur, A.; Bjerknes, R.; Sabaredzovic, A.; Bruserud, I. S.; Juliusson, P. B. Levels of per-and polyfluoroalkyl substances (PFAS) in Norwegian children stratified by age and sex-Data from the Bergen Growth Study 2. *International Journal of Hygiene and Environmental Health* **2023**, *252*, 114199.

(4) Leek, J. T.; Johnson, W. E.; Parker, H. S.; Jaffe, A. E.; Storey, J. D. J. B. The sva package for removing batch effects and other unwanted variation in high-throughput experiments. **2012**, *28* (6), 882-883.

(5) Di Tommaso, P.; Chatzou, M.; Floden, E. W.; Barja, P. P.; Palumbo, E.; Notredame, C. Nextflow enables reproducible computational workflows. *Nature biotechnology* **2017**, *35* (4), 316-319. DOI: 10.1038/nbt.3820 From NLM.

(6) Kim, D.; Paggi, J. M.; Park, C.; Bennett, C.; Salzberg, S. L. Graph-based genome alignment and genotyping with HISAT2 and HISAT-genotype. *Nature biotechnology* **2019**, *37* (8), 907-915.

(7) Harrow, J.; Frankish, A.; Gonzalez, J. M.; Tapanari, E.; Diekhans, M.; Kokocinski, F.; Aken, B. L.; Barrell, D.; Zadissa, A.; Searle, S. GENCODE: the reference human genome annotation for The ENCODE Project. *Genome research* **2012**, *22* (9), 1760-1774.

(8) Liao, Y.; Smyth, G. K.; Shi, W. featureCounts: an efficient general purpose program for assigning sequence reads to genomic features. *Bioinformatics (Oxford, England)* **2014**, *30* (7), 923-930. DOI: 10.1093/bioinformatics/btt656 From NLM.

(9) Kerimov, N.; Hayhurst, J. D.; Peikova, K.; Manning, J. R.; Walter, P.; Kolberg, L.; Samoviča, M.; Sakthivel, M. P.; Kuzmin, I.; Trevanion, S. J. A compendium of uniformly processed human gene expression and splicing quantitative trait loci. *Nature genetics* **2021**, *53* (9), 1290-1299.

(10) Hansen, K. D.; Irizarry, R. A.; Wu, Z. J. B. Removing technical variability in RNA-seq data using conditional quantile normalization. **2012**, *13* (2), 204-216.

(11) Beck, A. T. J. Manual for the beck depression inventory-II. **1996**.

(12) Spielberger, C. D.; Gonzalez-Reigosa, F.; Martinez-Urrutia, A.; Natalicio, L. F.; Natalicio, D. S. J. R. I. d. P. I. j. o. p. The state-trait anxiety inventory. **1971**, *5* (3 & 4).

(13) Watson, D.; Clark, L. A.; Tellegen, A. J. J. o. p.; psychology, s. Development and validation of brief measures of positive and negative affect: the PANAS scales. **1988**, *54* (6), 1063.

(14) John, O. P.; Donahue, E. M.; Kentle, R. L. J. J. o. P.; Psychology, S. Big five inventory. **1991**.

(15) Cloninger, C. R.; Przybeck, T. R.; Svrakic, D. M. J. P. r. The tridimensional personality questionnaire: US normative data. **1991**, *69* (3), 1047-1057.

(16) Delis, D. C. J. A. v. M. P. C. California verbal learning test. **2000**.

(17) Owen, A. M.; McMillan, K. M.; Laird, A. R.; Bullmore, E. J. H. b. m. N-back working memory paradigm: A meta-analysis of normative functional neuroimaging studies. **2005**, *25* (1), 46-59.

(18) Loring, D. W.; Martin, R. C.; Meador, K. J.; Lee, G. P. Psychometric construction of the Rey-Osterrieth Complex Figure: methodological considerations and interrater reliability. *Archives of*

clinical neuropsychology : the official journal of the National Academy of Neuropsychologists **1990**, *5* (1), 1-14. From NLM.
(19) Smith, A. *Symbol digit modalities test*; Western Psychological Services Los Angeles, 1973.
(20) David, N.; Bewernick, B. H.; Cohen, M. X.; Newen, A.; Lux, S.; Fink, G. R.; Shah, N. J.; Vogeley, K. J. J. o. c. n. Neural representations of self versus other: visual-spatial perspective taking and agency in a virtual ball-tossing game. **2006**, *18* (6), 898-910.
(21) Mogensen, U. B.; Grandjean, P.; Nielsen, F.; Weihe, P.; Budtz-Jørgensen, E. Breastfeeding as an exposure pathway for perfluorinated alkylates. *Environmental science & technology* **2015**, *49* (17), 10466-10473.
(22) Lederbogen, F.; Kirsch, P.; Haddad, L.; Streit, F.; Tost, H.; Schuch, P.; Wüst, S.; Pruessner, J. C.; Rietschel, M.; Deuschle, M. City living and urban upbringing affect neural social stress processing in humans. *Nature* **2011**, *474* (7352), 498-501.
(23) Van Donkelaar, A.; Martin, R. V.; Brauer, M.; Hsu, N. C.; Kahn, R. A.; Levy, R. C.; Lyapustin, A.; Sayer, A. M.; Winker, D. M. Global estimates of fine particulate matter using a combined geophysical-statistical method with information from satellites, models, and monitors. *Environmental science & technology* **2016**, *50* (7), 3762-3772.
(24) Zhu, Z.; Zhang, F.; Hu, H.; Bakshi, A.; Robinson, M. R.; Powell, J. E.; Montgomery, G. W.; Goddard, M. E.; Wray, N. R.; Visscher, P. M. J. N. g. Integration of summary data from GWAS and eQTL studies predicts complex trait gene targets. **2016**, *48* (5), 481-487.
(25) Burgess, S.; Thompson, S. G.; Collaboration, C. C. G. Avoiding bias from weak instruments in Mendelian randomization studies. *Int J Epidemiol* **2011**, *40* (3), 755-764. DOI: 10.1093/ije/dyr036.
(26) Verbanck, M.; Chen, C.-Y.; Neale, B.; Do, R. Detection of widespread horizontal pleiotropy in causal relationships inferred from Mendelian randomization between complex traits and diseases. *Nature genetics* **2018**, *50* (5), 693-698.
(27) Litkowski, E. M.; Logue, M. W.; Zhang, R.; Charest, B. R.; Lange, E. M.; Hokanson, J. E.; Lynch, J. A.; Vujkovic, M.; Phillips, L. S.; Hauger, R. L. Mendelian randomization study of diabetes and dementia in the Million Veteran Program. *Alzheimer's & Dementia* **2023**, *19* (10), 4367-4376.
(28) VanderWeele, T. J.; Ding, P. Sensitivity Analysis in Observational Research: Introducing the E-Value. *Ann Intern Med* **2017**, *167* (4), 268-274. DOI: 10.7326/m16-2607 From NLM.
(29) Burne, R. M.; Abrahamowicz, M. Adjustment for time-dependent unmeasured confounders in marginal structural Cox models using validation sample data. *Stat Methods Med Res* **2019**, *28* (2), 357-371. DOI: 10.1177/0962280217726800 From NLM.